

in the *electronic* contribution to the rate with driving force.^{62,63} Depending on the energy of the localized states, a misinterpretation of the data may result if T_{ab} is assumed constant. Future work will attempt to include a model for nuclear motion.

Conclusions

We have shown that semiempirical quantum chemical techniques predict the dependence of tunneling matrix element on distance and linker geometry. The localized states used in these calculations must have the proper exponential decay in order to calculate meaningful rates. To the extent that the linkers create periodic potentials for the electrons, we are assured of obtaining

proper wave-function decay in these calculations. There are two major qualities of the method that make it especially appealing. It allows direct study of the effect of linker geometry on the electronic tunneling matrix element. The method also allows systematic study of the effect of donor and acceptor redox level on the electronic tunnelling matrix element. It is hoped that the synthesis of other rigidly linked, weakly interacting electron donor-acceptor molecules will provide further tests of this theory.

Acknowledgment. The authors are grateful to Dr. N. Agmon, Dr. R. A. Marcus, Mr. J. N. Onuchic, and Dr. M. A. Ratner for very helpful suggestions with regard to this manuscript. This research was supported in part by NSF Grant No. DMR-8107494.

(62) Marcus, R. A.; Siders, P. *J. Phys. Chem.* **1982**, *86*, 622-630.
 (63) Beitz, J. V.; Miller, J. R. *J. Chem. Phys.* **1979**, *71*, 4579-4595.

Registry No. I, 76723-23-4; II, 81205-53-0; III, 81205-54-1; IV, 88548-86-1.

Bonded and Nonbonded Charge Concentrations and Their Relation to Molecular Geometry and Reactivity

R. F. W. Bader,* P. J. MacDougall, and C. D. H. Lau

Contribution from the Department of Chemistry, McMaster University, Hamilton, Ontario, Canada L8S 4M1. Received August 12, 1983

Abstract: The Laplacian of the charge density, the quantity $\nabla^2\rho(\mathbf{r})$, determines the regions of space wherein electronic charge is locally concentrated and depleted. This function demonstrates, without recourse to any orbital model or arbitrary reference state, the existence of local concentrations of electronic charge in both the bonded and nonbonded regions of an atom in a molecule. The form of the Laplacian of ρ for an isolated atom reflects its shell structure by exhibiting a corresponding number of pairs of spherical shells of alternating charge concentration and charge depletion. The uniform valence shell of charge concentration is distorted upon chemical combination through the creation of local maxima within this shell. The numbers, locations, and relative sizes of the bonded and nonbonded concentrations of charge in the valence shell of a bonded atom as determined by the Laplacian of ρ are found to be in general agreement with the corresponding properties that are ascribed to bonded and nonbonded electron pairs in models of electronic structure and, particularly, in Gillespie's VSEPR model of molecular geometry. Examples are considered which contain three (SO_2), four (CH_4 , SiH_4 , NH_3 , PH_3 , OH_2 , SH_2 , NF_3 , PF_3 , ClCl_2^+ , ClF_2^+), five (ClF_3 , SF_4 , SF_4O), and six (ClF_5) local concentrations of electronic charge in the valence shell of the central atom. It is also shown that the regions of maximum electronic charge concentration and depletion as determined by the Laplacian of ρ correlate respectively with the positions of electrophilic and nucleophilic attack. Nucleophilic attack at a carbonyl carbon, for example, is predicted to occur from above or below the plane of the nuclei along lines of approach forming an angle of $\sim 110^\circ$ with the $\text{C}=\text{O}$ bond axis. The Laplacian of ρ gives physical expression to the electron-pair concept of Lewis. This same function relates the local form of the charge density to the mechanics which govern it. Thus one may attempt through its use to obtain a deeper understanding of the models of molecular geometry and reactivity that make use of the electron-pair concept.

I. Introduction

The gradient vector field of the charge density, the field $\nabla\rho(\mathbf{r})$, determines the structure and structural stability of a molecular system.¹ In terms of the *global* behavior of this field, one may define the atoms² and the set of atomic interactions present in a molecule.^{3,4} The Laplacian distribution of the charge density, the field $\nabla^2\rho(\mathbf{r})$, identifies the regions of space wherein the electronic charge of a molecule is locally concentrated and depleted.⁵ The Laplacian of $\rho(\mathbf{r})$, as well as providing this enhanced view of the *local* form of the charge density, relates this form to

the quantum mechanical equations which govern the behavior of $\rho(\mathbf{r})$.^{6,7} In particular, the sign of the Laplacian of $\rho(\mathbf{r})$ determines the relative magnitudes of the local contributions of the potential and kinetic energy densities to their virial theorem averages. By obtaining a map of those regions where $\nabla^2\rho(\mathbf{r}) < 0$, the regions where electronic charge is concentrated, one obtains a map of the regions where the potential energy makes its dominant contributions to the energy of a system.⁵

The Laplacian distribution of a molecular charge distribution demonstrates the existence of local concentrations of electronic charge in both the bonded and nonbonded regions of an atom in a molecule. This information is obtained without recourse to any orbital model or arbitrary reference state. The ability to locate

(1) Bader, R. F. W.; Nguyen-Dang, T. T.; Tal, Y. *Rep. Prog. Phys.* **1981**, *44*, 893-948.

(2) Bader, R. F. W.; Beddall, P. M. *J. Chem. Phys.* **1972**, *56*, 3320-3329.

(3) Bader, R. F. W.; Anderson, S. G.; Duke, A. J. *J. Am. Chem. Soc.* **1979**, *101*, 1389-1395.

(4) Bader, R. F. W.; Nguyen-Dang, T. T.; Tal, Y. *J. Chem. Phys.* **1979**, *70*, 4316-4329.

(5) Bader, R. F. W.; Essén, H. *J. Chem. Phys.*, in press.

(6) Bader, R. F. W.; Nguyen-Dang, T. T. *Adv. Quantum Chem.* **1981**, *14*, 63-124.

(7) Bader, R. F. W.; Essén, H. "Local Density Approximations in Quantum and Solid State Physics"; Dahl, J. P., Avery, J., Eds.; Plenum Press: New York, 1983.

concentrations of negative charge is a property unique to the Laplacian of $\rho(\mathbf{r})$. The charge density itself exhibits local *maxima* only at the positions of nuclei and, aside from these, local *concentrations* of charge are not evident in $\rho(\mathbf{r})$ itself. The Laplacian of a scalar function measures its "lumpiness":⁸ in the present case, the tendency for the electronic charge to "lump together" at any point. The numbers, locations, and relative sizes of the bonded and nonbonded *charge concentrations* in the valence shell of an atom in a molecule as determined by the Laplacian of $\rho(\mathbf{r})$ are found to be in general agreement with the corresponding properties that are ascribed to the bonded and nonbonded *localized electron pairs* in Gillespie's VSEPR (valence-shell electron-pair repulsion) model of molecular geometry.⁹ With the model of localized electron pairs, which in general does not apply to the valence shells of atoms, replaced by the measured properties of local concentrations of electronic charge as determined by the Laplacian of $\rho(\mathbf{r})$, one may test the tenets of the VSEPR model to obtain a physical basis for the model and its predictions of molecular geometry.

As well as providing a model of molecular geometry based upon the properties of $\rho(\mathbf{r})$, the Laplacian of $\rho(\mathbf{r})$ may be used to obtain a charge density model of reactivity. It is shown that the local minima and maxima in $\nabla^2\rho(\mathbf{r})$, the regions of maximum electronic charge concentration and depletion, correlate respectively with the positions of electrophilic and nucleophilic attack in a molecule.

II. Properties of the Laplacian of $\rho(\mathbf{r})$

The determination of the regions wherein a scalar field is concentrated throughout three-dimensional space is a nontrivial problem. The answer is provided by the properties of the Laplacian of the distribution as given in terms of its three competing curvatures at each point in space:

$$\nabla^2\rho(\mathbf{r}) = \frac{\partial^2\rho}{\partial x^2} + \frac{\partial^2\rho}{\partial y^2} + \frac{\partial^2\rho}{\partial z^2}$$

It is important that one have a clear understanding of "lumpiness" in a charge density as determined by $\nabla^2\rho$, in the face of the observation that such lumps are not apparent in ρ itself. In one dimension the curvature of $\rho(\mathbf{r})$ is a measure of the difference between the average value of ρ at points neighboring \mathbf{r} and its value at \mathbf{r} . This follows⁸ from the fundamental definition of the derivative

$$\lim \{\rho(x) - \frac{1}{2}[\rho(x-dx) + \rho(x+dx)]\} = -\frac{1}{2} \lim \{[\rho(x+dx) - \rho(x)] - [\rho(x) - \rho(x-dx)]\} = -\frac{1}{2}(d^2\rho/dx^2)(dx)^2$$

Thus if $d^2\rho/dx^2 < 0$, ρ at x is larger than the average of ρ at $x+dx$ and $x-dx$ and ρ will have a downward curvature at that point when plotted against x .

Consider a spherical surface of constant density in an atom. An axis through the nucleus, say the z axis, is normal to the surface and intersects it at the point $(0, 0, z)$. The charge density increases with decreasing z and hence $\partial\rho/\partial z < 0$ and, in general, the curvature along such a radial line is found to be positive, $\partial^2\rho/\partial z^2 > 0$. Thus $\rho(0, 0, z)$ is less than the average of its values at the points $(0, 0, z \pm dz)$. The charge density is, however, a maximum at $(0, 0, z)$ in the tangent plane, $\partial\rho/\partial x = \partial\rho/\partial y = 0$, and the corresponding curvatures are negative. Thus $\rho(0, 0, z)$ is greater than the average of its values at $(\pm dx, 0, z)$ and $(0, \pm dy, z)$ (see Figure 1). If the sum of the magnitudes of the two negative (perpendicular) curvatures exceeds the value of the positive (parallel) curvature, $\nabla^2\rho(0, 0, z) < 0$. In such a case the value of $\rho(0, 0, z)$ is greater than the value of ρ obtained by averaging over *all* points in the neighborhood of $(0, 0, z)$. The charge density and hence electronic charge are concentrated at this point relative to their values averaged over all neighboring points. By determining a radius in an atom at which $\nabla^2\rho(\mathbf{r})$ is a minimum (or a maximum), one determines a radius at which electronic charge

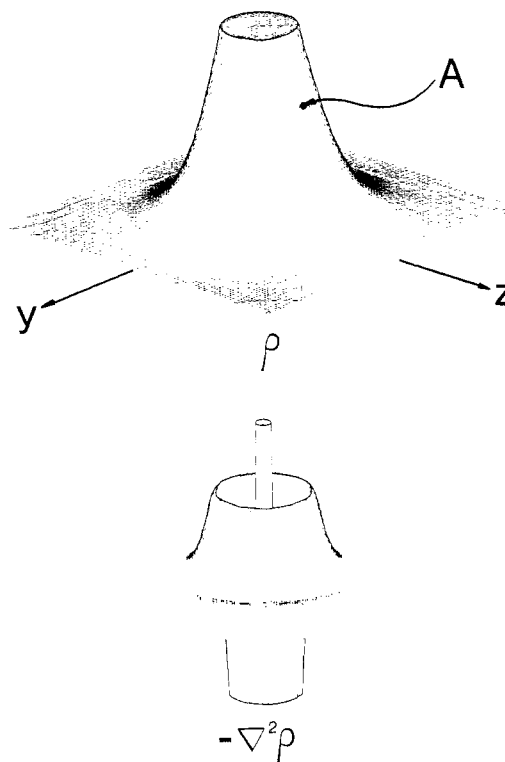


Figure 1. The values of the charge density ρ and $-\nabla^2\rho$ are plotted on the third axis for a plane containing the nucleus of an oxygen atom. The point A (see text) denotes a value of ρ for a point on the z axis. At this point the curvature of ρ along z , the curvature parallel to a radial line, is positive, while its curvature along the y axis, a perpendicular curvature, is negative, as it also is along the x axis. If the sum of the magnitudes of the two perpendicular curvatures exceeds the value of the parallel curvature, $\nabla^2\rho < 0$ and $-\nabla^2\rho$ indicates that electronic charge is locally concentrated at the point in question. The circular maximum in $-\nabla^2\rho$ is a two-dimensional slice through the sphere of valence-shell charge concentration for the oxygen atom. The radial distance of this maximum defines r_A for the oxygen atom (see Table I). In this and succeeding similar displays of ρ and $-\nabla^2\rho$ both functions are arbitrarily terminated and the large magnitudes they attain in the region of a core are not shown.

is maximally concentrated (or depleted).¹⁰

The observation that ρ exhibits a maximum at a nuclear position does not imply that the contraction of ρ toward a nucleus is the dominant one at all distances from a nucleus, even in an isolated atom. Indeed this cannot be so, for the atomic integral of $\nabla^2\rho(\mathbf{r})$ for a free or a bound atom^{2,6} must vanish. Thus in addition to regions where the contraction of ρ along radial lines toward the nucleus is dominant and $\nabla^2\rho > 0$, there must exist a region or regions where the magnitudes of the curvatures of ρ perpendicular to these radial lines are dominant, yielding negative values for the Laplacian of ρ (see Figure 1). Thus $\nabla^2\rho(\mathbf{r})$ exhibits spherical nodes in an atom and their number is related to its shell structure.⁵ There are pairs of regions, one negative and one positive, for each principal quantum shell with the innermost region where ρ is a local maximum being negative. The first spherical node in a one-electron atom occurs at $r = 1/Z$ (Z = nuclear charge), and this is very nearly true for many-electron atoms as well, becoming increasingly exact as Z increases. The second spherical node for the elements Li \rightarrow Ne is found at a value of r a few tenths of an atomic unit greater than the radius of the core. Thus one may associate pairs of regions, one negative, and one positive, with each shell including the valence shell. The result is a series of layered

(8) Morse, P. M.; Feshbach, H. "Methods of Theoretical Physics", Part I; McGraw-Hill: New York, 1953.

(9) Gillespie, R. J. "Molecular Geometry"; Van Nostrand-Reinhold: London, 1972. Gillespie, R. J. *Angew. Chem.* 1967, 6, 819-830.

(10) In the region of the valence shell where $\nabla^2\rho < 0$ in third-row atoms such as sulfur and chlorine, the parallel curvature becomes small in magnitude and negative over a small radial distance. In such a case all three curvatures of ρ are negative, but since $\nabla\rho \neq 0$ (the derivative of ρ parallel to a radial line does not vanish), the charge distribution does not possess a local maximum but does exhibit a shoulder.

Table I. Properties of Valence-Shell Sphere of Charge Concentration for Spherical Atoms^a

atom	state	$r_A,^b \text{ \AA}$	$-\nabla^2\rho, \text{ au}^c$	μ_3^d
Li	² S	1.320	0.002	0.015
Be	¹ S	0.843	0.027	0.574
B	² P	0.629	0.141	5.27
C	³ P	0.498	0.506	29.7
N	⁴ S	0.411	1.447	123.
O	³ P	0.348	3.480	409.
F	² P	0.301	7.592	1180.
Ne	¹ S	0.265	15.285	3020.

^a All results calculated from atomic wave functions expanded in a Slater basis: Clemente, E.; Roetti, C. *At. Data Nucl. Data Tables* 1974, 14, 177. ^b Radius of sphere. ^c 1 au of $\nabla^2\rho = e/a_0^5 = 24.100 \text{ e/\AA}^5$. ^d Radial curvature.

volumes in which the dominant contractions in ρ alternate between those parallel to and those perpendicular to the radial lines originating at the nucleus. In particular, the Laplacian of ρ defines the chemically important valence-shell charge concentration.

The shell structure in $\nabla^2\rho$ for an atom is illustrated in Figure 1. In this and the following three-dimensional displays of the Laplacian of ρ , the function plotted is $-\nabla^2\rho(\mathbf{r})$, thereby transforming the minima in the Laplacian into maxima in concentrations of electronic charge. A program has been written which finds the critical points in $\nabla^2\rho$, points where $\nabla(\nabla^2\rho) = 0$, and determines the eigenvalues of the Hessian of $\nabla^2\rho$ (the curvatures of $\nabla^2\rho$) at each critical point. Each critical point is classified by the number of nonzero eigenvalues (its rank) and the algebraic sum of the signs of the eigenvalues (its signature). A minimum in $-\nabla^2\rho$, a local depletion of charge, exhibits three positive curvatures and it is a (3, +3) critical point. A maximum in $-\nabla^2\rho$, a local concentration of charge, is a (3, -3) critical point, and saddle points may be either (3, +1) or (3, -1) critical points.

In an atom there is a local maximum in $-\nabla^2\rho$ (a maximum of charge concentration in Figure 1) at the position of the nucleus. The negative of the Laplacian of ρ also attains a maximum value on a spherical surface (for a sphericalized atomic density) in each succeeding quantum shell present in the atom.¹¹ Thus for atoms other than hydrogen and helium, which exhibit only the local maximum at the nucleus, the Laplacian of ρ defines the radius of a sphere within the valence-shell charge concentration on which the valence charge density is maximally concentrated. Table I lists the values of these radii, r_A , for the atoms $A = \text{Li} \rightarrow \text{Ne}$.

The spherical shells of charge concentration and depletion defined by $\nabla^2\rho$ yield a three-dimensional analogue of the maxima and minima in the one-dimensional radial distribution function of an atom. This shell structure in $\nabla^2\rho$ for an isolated atom is disturbed upon chemical combination. The disturbance is such that local maxima and minima are created in the valence-shell charge concentration of the atom. The Laplacian of the charge density thus recovers in terms of a property of ρ , the local concentrations of negative charge whose existence has been previously assumed by chemists on the basis of localized electron pair and localized orbital models of electronic structure. The manner in which the valence-shell charge concentration in the oxygen atom (Figure 1) is distorted upon chemical combination is illustrated in Figure 2 which portrays the charge density and its Laplacian for the two symmetry planes of the water molecule. In the plane perpendicular to the plane of the nuclei (Figure 2a), $\rho(\mathbf{r})$ exhibits a single maximum at the position of the oxygen nucleus, and thus $\rho(\mathbf{r})$ itself offers no direct evidence to support a model that assumes the existence of two localized nonbonded electron pairs. Contained in the small departures from circular symmetry in $\rho(\mathbf{r})$, however, are variations in its local curvatures, and the corresponding display of the Laplacian of ρ shows, in a rather dramatic fashion, the existence of two local concentrations of electronic charge density in the valence shell of the oxygen atom (compare with Figure 1).

(11) Each point on such a surface is a (1, -1) critical point; two of the curvatures of $-\nabla^2\rho$ are zero and the third curvature, the one along a radial line, is negative.

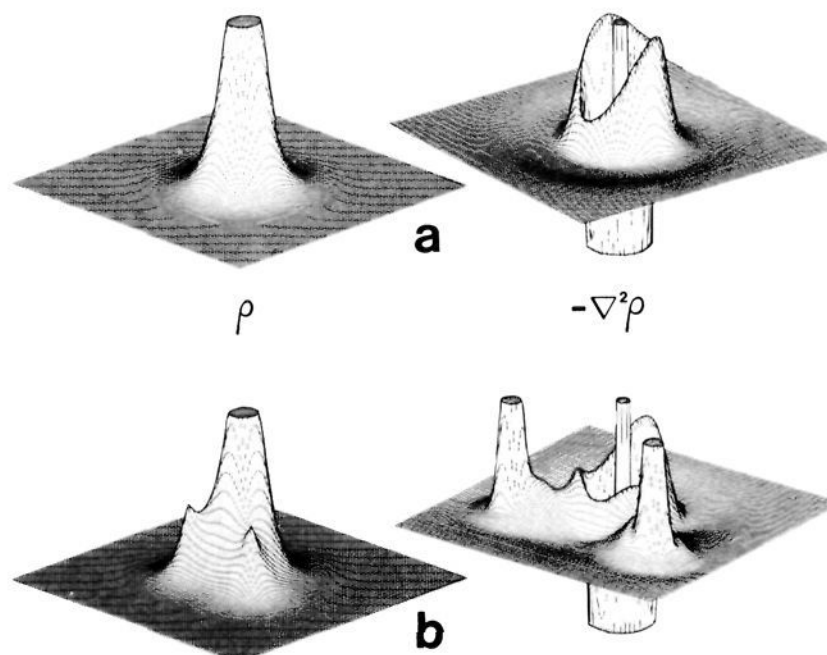


Figure 2. The values of ρ and $-\nabla^2\rho$ plotted on the third axis for the two symmetry planes of the water molecule. In the nonbonded plane, ρ exhibits a single local maximum at the position of the oxygen nucleus. In this same plane the valence-shell charge concentration exhibits two local maxima (two (3, -3) critical points in $-\nabla^2\rho$) of charge concentration and two saddle points in $-\nabla^2\rho$. In the plane of the nuclei, ρ exhibits a local maximum at each of the nuclei, as does $-\nabla^2\rho$. In addition, the valence-shell charge concentration of the oxygen atom also exhibits two local maxima, one along each of the bond paths linking the protons to oxygen. What appears as a third maximum in this shell is not a local maximum, but another view of the (3, -1) saddle point between the two nonbonded maxima. The value of $-\nabla^2\rho$ at this saddle point is less than its value at the nonbonded maxima (see top diagram). Thus the bottom diagram makes clear the general observation that bonded charge concentrations are smaller than nonbonded concentrations. The two diagrams illustrate that the uniform sphere of charge concentration of an oxygen atom is transformed into a shell which exhibits four local maxima and four intervening saddle points. Each saddle point possesses at least one axis in the shell along which $-\nabla^2\rho$ is a local minimum.

In the plane of the nuclei, Figure 2b, $\rho(\mathbf{r})$ again exhibits maxima only at the positions of the nuclei and ridges linking the oxygen nucleus to the protons, indicating the presence of two (3, -1) or bond critical points.^{1,3} The Laplacian of ρ , on the other hand, exhibits two local concentrations of negative charge in the valence shell of the oxygen atom in addition to those at the positions of the nuclei. The valence-shell charge concentration of an oxygen atom bonded to two hydrogen atoms thus exhibits four local maxima in $-\nabla^2\rho$, i.e., four local concentrations of electronic charge: two bonded concentrations (each lies on a bond path linking the oxygen to a hydrogen nucleus), forming an angle 103.1° with the oxygen nucleus, and two nonbonded concentrations, forming a corresponding angle of 138.3° .

While the pattern of bonded and nonbonded charge concentrations defined by the Laplacian of ρ mimic in some respects the spatial properties of equivalent or localized molecular orbitals, the two descriptions are not to be equated, one to the other. Lennard-Jones¹² defined equivalent orbitals to obtain a localized and directed description of a chemical bond from molecular orbital theory. Through a suitable orthonormal transformation, as determined by the symmetry of the system, the canonical, i.e., delocalized, molecular orbitals were transformed into symmetrically equivalent sets of orbitals, each orbital exhibiting a maximum value coincident with a given bond direction. In this sense, the equivalent orbitals were spatially localized, and they thus provided a link between molecular orbital theory and the concept of the localized electron pair bond as developed from the ideas of Lewis and valence-bond theory. In subsequent papers with Pople,¹³ it was demonstrated that the equivalent orbital description of the bonded pairs of a system such as water or

(12) Lennard-Jones, J. E. *Proc. R. Soc. London, Ser. A* 1949, 198, 1-14, 14-26.

(13) Lennard-Jones, J. E.; Pople, J. A. *Proc. R. Soc. London, Ser. A* 1950, 202, 166-180; Pople, J. A. *Q. Rev. Soc. London* 1957, 11, 273.

ammonia led in a natural way to a corresponding localized description of the unshared or lone pairs of electrons.

The original papers by Lennard-Jones and Pople stressed that since the total wave function and the derived physical properties of the system, such as total electronic charge density $\rho(\mathbf{r})$, were invariant to an orthonormal transformation of the orbital set, the particular choice of an equivalent set was arbitrary. Hence, the associated picture of localized pairs of electrons was itself an arbitrary description of the system. Lennard-Jones¹⁴ in particular was careful to point out that the possibility of representing the electronic structure of a system in terms of equivalent orbitals which exhibited some degree of spatial localization did not itself imply the existence of spatially localized pairs of electrons. He noted that the degree to which pairs of electrons are spatially localized is determined by the quantum mechanical pair distribution function and not by a particular orbital representation of the charge density. Thus, the ability to express the total charge density in terms of a sum of localized orbital densities does not imply the existence of localized pairs of electrons.

In general, the extent of spatial pairing and localization of electrons as determined by the properties of the quantum mechanical pair density do not correspond to the idealized pictures associated with the electron-pair concept. The complete localization of N electrons to some region of real space demands that their Fermi correlation be totally contained within the same region of space, i.e., that the double integration of the density of the Fermi hole over the region yield a value of $-N$.¹⁵ In such a case there is no exchange of the electrons in the region with electrons in other regions. This limiting situation is approached for spherical core-like regions centered on nuclei. Such regions may be defined in terms of an extremum principle, being bounded by a surface such that the contained Fermi correlation is *maximized*. This corresponds to finding a region for which the fluctuation in the average electron population is a minimum and in which the electron number and pair densities are maximally localized.¹⁵ Such core regions in general exist and are *found* to possess an average population of approximately two electrons.¹⁶ The same spatially localized pairing of electrons is also significant in some simple ionic systems such as LiH, BeH₂, and BH₃, which contain one, two, or three pairs of electrons in the neighborhood of a single core. These same systems are well described by the loge model of Daudel¹⁷ which supposes some most probable division of space yielding localized pairs of electrons. When the pair density does exhibit localization, it is reflected in a rapid change of slope in $\rho(\mathbf{r})$ on the boundary of the region or in the existence of a surface of zero flux in $\nabla\rho(\mathbf{r})$.¹⁵

The requirement for perfect spatial pairing is not that each member of a set of orbitals be spatially localized, but that they each be localized to separate regions of real space.¹⁵ Reference to displays of localized orbitals shows that when four or more localized orbitals are associated with a given nucleus, the condition of separate spatial localization is not met to a significant degree. In a very physical sense, there is room to "pack" separately three and even four pairs of electrons around cores containing a Be or B nucleus, but for cores containing the carbon to neon, the net attractive force exerted on the valence electrons is so great (the charge density is so contracted toward the core) that the pairs are drawn strongly together and are no longer physically distinct. Thus it is not possible to find surfaces enclosing valence regions in nonionic systems such as CH₄, H₂O, NH₃, or HF which maximize the contained Fermi correlation, and there is no physical localization of the valence charge in these molecules.¹⁵ Bearing

in mind the demonstrated limited applicability of the localized electron-pair and localized orbital models, it is proposed that the maxima present in the negative of the Laplacian of ρ be labeled for what they are—bonded and nonbonded charge concentrations.

III. Electronic Charge Concentrations and Models of Molecular Geometry

The valence-shell electron pair repulsion theory of Gillespie^{9,18} is the most successful and widely used model for the prediction of geometries of closed-shell molecules. This theory assumes that the stereochemistry in the neighborhood of a central atom A is determined primarily by the repulsions between electron pairs in its valence shell. Initially one does not distinguish between bonded and nonbonded pairs and one simply determines the most probable arrangement of all the pairs on the surface of a sphere by maximizing the least distance between any two pairs. If all the pairs are bonded and equivalent, this most probable arrangement determines the stereochemistry. Nonbonded pairs are assumed to be more diffuse and space filling than bonded pairs and to exert a larger repulsive force on other pairs. Thus the symmetry of the most probable arrangement is lowered if nonbonded pairs are present. If there are inequivalent sites in the most probable arrangement, the nonbonded pairs occupy those sites which keep them most separated from other pairs (ClF₃, for example, is T-shaped with the two nonbonded pairs occupying equatorial sites in a trigonal-bipyramidal arrangement).

In the comparison of Gillespie's model with the properties of the Laplacian of ρ , it is useful to replace the spherical surface on which the hypothetical electron pairs are assumed to be localized in Gillespie's model with the valence shell of charge concentration as defined by $-\nabla^2\rho$ and, similarly, to replace the localized pairs themselves with the local concentrations of negative charge present in this shell. Also of importance to Gillespie's model are the relative sizes of the bonded and nonbonded pairs. Estimates of the relative spatial extent of the bonded and nonbonded charge concentrations may be obtained in the following manner. Saddle points, as well as local maxima, are present in the valence shell of maximum charge concentration for a bonded atom. Each critical point of $-\nabla^2\rho$ in this shell possesses one negative curvature along a line radially directed from the nucleus; $-\nabla^2\rho$ reaches a maximum value at the critical point along a radial line in this shell. Thus the properties of each critical point may be summarized by giving the two curvatures in the plane tangent to the shell of maximum charge concentration. Neighboring maxima, (2, -2) critical points, are separated by an intervening saddle point, a (2, 0) critical point. Trajectories of $\nabla(-\nabla^2\rho)$ which terminate at these saddle points partition the surface of the valence sphere into separate domains, each domain containing a single maximum. (This two-dimensional partitioning by the field $\nabla(-\nabla^2\rho)$ is analogous to the partitioning of three-dimensional space into atomic basins by the field $\nabla\rho$.)¹ Figure 3 contains a display of $\nabla^2\rho$ for NH₃ and PH₃. In each case the positions of the nonbonded and one of the bonded maxima in $-\nabla^2\rho$ are indicated as are the positions of intervening saddle points. To map out the exact topological boundaries on the surface of maximum charge concentration would be a difficult task. Instead the surface area of each charge concentration is approximated by the portion of the surface of a sphere with a radius equal to the distance of the maximum from the nucleus and bounded by a cone subtending an angle α at the nucleus as determined by the neighboring saddle points in $-\nabla^2\rho$ (see diagrams for NH₃ and PH₃ in Figure 3). A relative measure of the radial "thickness" of a charge maximum is given by μ_3 , the value of the radial curvature of $\nabla^2\rho$.

Valence-Shell Charge Concentrations with Three and Four Maxima. We begin with an investigation of the Laplacian of ρ for the hydrides AH_n, A = C, N, and O, all of which are assumed to possess four pairs of electrons in the valence shell of A. The properties of the bonded and nonbonded charge concentrations in these molecules are given in Table II, calculated from wave functions and optimized geometries obtained from the 6-31G**

(14) Lennard-Jones, J. E. *J. Chem. Phys.* **1952**, *20*, 1024-1029.

(15) Bader, R. F. W.; Stephens, M. E. *J. Am. Chem. Soc.* **1975**, *97*, 7391-7399.

(16) The term core as used in this paper is defined in this manner. Some values of average core populations \bar{N} , their radii r , and their % localizations are 2.0, 0.28 Å, and 88% for carbon; 2.0, 0.14 Å and 77% for neon; 10.1, 0.40 Å and 80% for the combined K and L shells of Ar.

(17) Daudel, R. *C.R. Acad. Sci. Paris* **1953**, *237*, 601. Daudel, R. "The Fundamentals of Theoretical Chemistry"; Pergamon Press: Oxford, 1968. Daudel, R.; Bader, R. F. W.; Stephens, M. E.; Borrett, D. S. *Can. J. Chem.* **1974**, *52*, 1310-1320.

(18) Gillespie, R. J. *J. Am. Chem. Soc.* **1960**, *82*, 5978-5983.

Table II. Bonded and Nonbonded Charge Concentrations in AH_n ^a

AX_n	$R(AH)$ (calcd), Å	$\angle HAH$ (calcd), deg	bonded charge concentrations				nonbonded charge concentrations				net charge on H			
			r_A , Å	$-\nabla^2\rho$, au ^b	$\angle bAb$, deg	area, Å ²	μ_3	$\angle nAb$, deg	r_A , Å	$-\nabla^2\rho$, au ^b		$\angle nAn$, deg	area, Å ²	μ_3
CH ₄	1.082	109.5	0.537	0.717	109.5	0.91	10.1							-0.06
NH ₃	1.001	107.6	0.434	1.911	106.6	0.48	77.7	112.3	0.388	3.210		0.74	236.5	+0.37
OH ₂	0.943	106.0	0.374	2.688	103.1	0.32	223.4	102.2	0.335	6.616	138.3	0.45	715.1	+0.62

^a All results calculated using the 6-31G** basis set. ^b 1 au of $\nabla^2\rho = e/a_0^3 = 24.100 e/\text{Å}^3$.

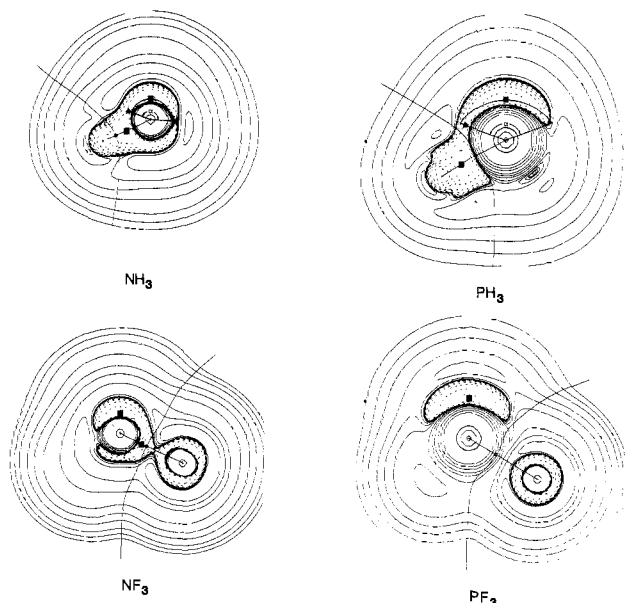


Figure 3. Contour maps of $\nabla^2\rho$ for NH_3 , NF_3 , PH_3 , and PF_3 . Each map is for a symmetry plane containing the N or P nucleus and an H or F nucleus. The diagrams are overlaid with the bond paths and interatomic surfaces as determined by the gradient vector field of ρ . Bond critical points in $\nabla\rho$ are denoted by black circles. The positions of the local charge concentrations ($(3, -3)$ critical points in $-\nabla^2\rho$) are denoted by black squares. The values of $|\nabla^2\rho|$ at these local maxima are given in Table III. Dashed contours denote negative, solid contours positive values of $\nabla^2\rho$. The determination of the surface area associated with a local charge concentration through the definition of a cone subtending an angle α at the A nucleus is illustrated for the nonbonded maxima on N and P in their hydrides. The black triangles denote the positions of saddle points in the valence-shell charge concentrations of N and P in these two molecules. The ionic nature of the binding in PF_3 is evident in the separate localization of the regions of charge concentration within the basins of the F and P atoms. The F distribution approaches the shell structure characteristic of an isolated F ion. In NH_3 and to a lesser extent in NF_3 , $\nabla^2\rho$ is negative along the bond path and charge is concentrated between the nuclei and shared by both. The contour values in au are ± 0.002 , ± 0.004 , and ± 0.008 increasing in powers of 10 to ± 8.0 . The outermost contour in each plot is 0.002 au.

basis set. In each case the valence-shell charge concentration exhibits four local maxima in $-\nabla^2\rho$, but is no longer spherical as it was in the free atom. The radial distance r_A of a bonded charge concentration is increased by 0.02 to 0.04 Å over the value of the radius of the sphere of maximum charge concentration present in the free atom, while the nonbonded charge concentrations are drawn slightly closer to the A nucleus. (Compare the r_A values for the bonded and nonbonded maxima given in Table II with the corresponding value of r_A for the free atom in Table I.) The magnitude of $\nabla^2\rho$ is considerably greater for a nonbonded maximum than it is for a bonded maximum. Thus charge is concentrated to a greater extent in the nonbonded than in the bonded maxima. The curvature of $\nabla^2\rho$ perpendicular to the surface of charge concentration, μ_3 , is always greater for the nonbonded than for the bonded charge concentrations. Thus the nonbonded charge concentrations are "thinner" in radial extent than are the bonded ones. These observations, which are understandable in terms of Gillespie's⁹ argument that a nonbonded charge concentration is attracted by a single

nucleus while a bonded one is attracted by, and shared between, two nuclei.

The transformation of a bonded into a nonbonded charge concentration on passage from CH_4 to NH_3 results in a decrease in the angle between two bonded charge concentrations, the angle bAb , and hence to an angle greater than tetrahedral between the nonbonded and bonded charge concentrations, the angle nAb . Correspondingly, the nonbonded charge concentration in NH_3 occupies a larger fraction of the surface of charge concentration than does a bonded one. Thus a nonbonded charge concentration, while radially more contracted than a bonded one, is laterally more diffuse and possesses a larger surface area. In H_2O where there are two nonbonded charge concentrations, the angle between the bonded concentrations is further reduced to 103° . This angle is to be compared with the angle formed by the nonbonded charge concentrations of 138° .

All of the observations regarding the minima in the Laplacian of ρ in the valence shell of the central atom in CH_4 , NH_3 , and H_2O are in accord with the tenets of VSEPR theory. The primary observation is that of the presence of four local concentrations of charge in the valence shell of atom A. A nonbonded charge concentration occupies a larger fraction of the surface of charge concentration than does a bonded concentration, and the angle subtended at the A nucleus by two nonbonded concentrations is greater than the corresponding angle formed by two bonded concentrations in an equilibrium geometry.

We now consider the changes incurred by replacing A with a neighboring element from the same family of the periodic table. Since we are restricted to the use of the 6-21G* basis set¹⁹ in the description of third-row atoms, all of the examples listed in Table III are calculated from wave functions and optimized geometries obtained by using the 6-21G* or 6-21G** basis sets. By comparing the results for H_2O and NH_3 given in Tables II and III, one sees that no qualitative changes in the properties of the Laplacian of ρ result from this change in basis set. In all comparisons the calculated changes in bond lengths and bond angles agree with the experimentally observed trends.

The radial distances of the nonbonded charge concentrations from the A nucleus are approximately doubled on changing from N to P and O to S for the same ligand. These increases are consequences of the greater core size of a third-row as compared to a second-row element. The changes in radial distances of the bonded charge concentrations found for the substitution of silicon for carbon and phosphorus for nitrogen are exceptionally large because of the significant degree of charge transfer from A to H in SiH_4 and PH_3 compared with their second-row counterparts (see Table III).²⁰ In systems where the competition for the bonded charge density is less one-sided and where r_A can still be viewed as a property characteristic of atom A, the increase in the bonded radius r_A resulting from the increased core size is nearly equal

(19) Binkley, J. S.; Pople, J. A.; Hehre, W. J. *J. Am. Chem. Soc.* **1980**, *102*, 939-947. Gordon, M. S.; Binkley, J. S.; Pople, J. A.; Pietro, W. J.; Hehre, W. J. *Ibid.* **1982**, *104*, 2797-2803.

(20) The net charges on the atoms are determined by integrating $\rho(r)$ over the basin of an atom (the region of space encompassed by the atom's atomic surface) and subtracting this number from its nuclear charge. The transfer of charge from Si \rightarrow H, 0.7 e, is so large that only a single maximum in $-\nabla^2\rho$ is found along each Si-H bond path, with the maximum at the position of the proton. In the other hydrides a bonded maximum is found in the valence-shell charge concentration of A in addition to the maximum always present at the position of the proton. In PH_3 the valence shell of P is stretched out into the basin of the H atom and the P-H bonded maximum lies within the basin of the H atom.

Table III. Bonded and Nonbonded Charge Concentrations on A in AX_n^a

AX _n	R(AX) (calcd), Å	∠XAX (calcd), deg	bonded charge concentrations					nonbonded charge concentrations					net charge on X		
			r _A , Å	-∇ ² ρ, au	∠bAb, deg	area, Å ²	μ _s , au	∠nAb, deg	r _A , Å	-∇ ² ρ, au	∠nAn, deg	area, Å ²		μ _s , au	
CH ₄	1.087	109.5	0.612	1.158	109.5	0.99	6.2								-0.04
SiH ₄	1.477	109.5		charge transfer to hydrogen											-0.74
NH ₃	1.007	105.7	0.510	1.685	104.4	0.71	19.5	114.2	0.388	2.299		1.12	100.0		+0.34
PH ₃	1.408	95.4	0.945	0.638	96.1	1.61	2.5	120.8	0.775	0.325		2.49	7.8		-0.63
OH ₂	0.947	103.8	0.441	2.057	101.0	0.38	51.4	104.4	0.339	4.138	134.0	0.50	210.1		+0.56
SH ₂	1.330	94.3	0.841	0.806	95.4	1.17	4.4	105.4	0.696	0.554	133.7	2.20	17.3		-0.34
NF ₃	1.337	102.5	0.473	0.990	97.6	0.45	28.2	119.6	0.358	4.450	119.6	0.70	294.7		-0.36
PF ₃	1.548	97.5		charge transfer to fluorine											-0.90
ClCl ₂ ⁺	2.002	106.3	0.653	0.717	104.3	1.48	25.3	101.9	0.615	1.148	140.9	1.88	48.9		
ClF ₂ ⁺	1.576	100.2	0.658	0.671	99.0	0.66	27.9	102.0	0.604	1.541	142.8	1.84	62.2		-0.18
S				charge transfer to oxygen											
SO ₂	1.423	118.7							0.678	0.785		1.56	24.4		
O			0.426	1.769	124.0	1.82	54.1	118.0							
									0.346	3.697				182.0	-1.26

^a All results calculated using the 6-21G** basis set.

to the increase in calculated bonded length. In the pair SH₂-OH₂, for example, r_S - r_O = 0.400 Å and ΔR(AH) = 0.383 Å; in the pair OCl₂-SCl₂ (not listed in Table III), r_S - r_O = 0.318 Å and ΔR(AX) = 0.312 Å. The value of -∇²ρ at both the bonded and nonbonded maxima is approximately halved in passing from a second- to a third-row element. This observation is again a consequence of the increased core size and the subsequent reduction in the attractive force exerted on the valence charge by the A nucleus.

The decrease in the nuclear attractive force accompanying the increase in core size is also reflected in the dramatic increase in both the surface area and thickness of the nonbonded charge concentrations on P and S compared with N and O. This is illustrated in Figure 3 for the pair NH₃-PH₃. Gillespie⁹ has reasoned that for the elements in the third row, the bonded pairs do not interact with each other strongly until the angle between them approaches 90°. In the VSEPR model, the bond angle in PH₃ approaches 90° (∠HPH(exptl) = 93.3°) to accommodate the spreading out of the lone pair "around the 'surface' of the phosphorus atom".⁹ The presence of a second lone pair in H₂S causes a further reduction in the bond angle (∠HSH(exptl) = 92.2°). The angle bAb decreases along with the decrease in bond angle, but the angle between the nonbonded maxima (∠nAn) remains essentially unchanged from H₂O to H₂S. It must be borne in mind that the approximate doubling of the radius of the valence-shell charge concentration between second- and third-row elements leads to a near quadrupling of its surface area. Thus even though the angle bAb approaches 90° in the third-row hydrides, the actual distance between the bonded charge maxima is greater in H₂S than in H₂O (1.20 compared with 0.68 Å) and greater in PH₃ than in NH₃ (1.41 compared with 0.81 Å).

The remaining entries in Table III are to illustrate the effect of increasing electronegativity of the ligand on the bond angle. The general argument of VSEPR theory is that an increase in the electronegativity of the ligand causes a decrease in the size of the bonded pairs, a decrease in repulsion between them, and hence a decrease in the bond angle.^{9,18} This decrease in bond angle is illustrated by the pairs NH₃-NF₃ and ClCl₂⁺-ClF₂⁺. In some cases the presence or absence of nonbonded pairs of electrons on the ligands is used to rationalize exceptions to the above ligand electronegativity rule. The example considered here is the pair PF₃-PH₃. The regularly behaved examples are considered first.

The replacement by F of H in NH₃ and of the Cl ligands in ClCl₂⁺ results in a decrease in the degree of charge concentration in the bonded maxima, to a decrease in their surface area, and to a decrease in their radial thickness. In NF₃ there is also a significant decrease in the bonded radius. Thus as is evident in Figure 3, fluorine substitution causes the bonded maxima to decrease in magnitude and in spatial extent resulting in their closer approach as indicated by the decreased values for the angle bAb.

The nonbonded maxima, on the other hand, are increased in magnitude upon substitution by fluorine. They are also drawn closer to their respective nuclei and decreased in radial extent.

The overall effect of fluorine is to increasingly localize both the bonded and nonbonded charge concentrations and, because of its net negative charge, to polarize the charge distributions of nitrogen and chlorine into their nonbonded regions.

The molecule PF₃ differs from NF₃ and ClF₂⁺ in that it exhibits an extreme charge transfer to the fluorine atoms. The valence-shell charge concentration on phosphorus is reduced to a single maximum in its nonbonded region, the remaining concentrations of valence charge being *separately* localized on the fluorines. In atomic interactions involving significant charge transfer, the charge distributions of both the donor and acceptor are necessarily polarized in a direction counter to the direction of charge transfer. These polarizations are evident both in the charge density and in its Laplacian as shown in Figure 3. The fluorine charge distributions in PF₃ are best described as fluoride ion distributions polarized toward the positively charged phosphorus, which in turn is polarized away from the fluorines. The large bond angle in PF₃ compared with that in PH₃ could be ascribed to the repulsions between the negatively charged fluorine atoms or, alternatively, to a repulsion between their nonbonded pairs.

The two or three pairs of electrons forming a multiple bond are treated as a single entity in the VSEPR model.⁹ On this basis the final entry in Table III, sulfur dioxide, is considered to be a V-shaped molecule with two bonded pairs in each of two double bonds and a single nonbonded pair, in accord with the Lewis structure for this molecule.²¹

There is significant charge transfer from S to O in SO₂ resulting in a very polar atomic interaction. There is but a single bonded charge maximum along each bond path, and reference to Table III indicates that it exhibits the characteristic properties of a bonded maximum on oxygen. The only charge maximum in the valence shell of sulfur is found in its nonbonded region. Thus there are three charge concentrations in the neighborhood of the sulfur core, two bonded and one nonbonded, but the bonded concentrations are in the valence shells of the oxygen atoms which, as anticipated on the basis of the Lewis structure for this molecule, also possess two nonbonded charge concentrations. The charge concentration of the S=O bond is contiguous over the valence shells of both atoms, and it is spread over a relatively large area of the surface of charge concentration of the sulfur atom, particularly in the plane perpendicular to the plane of the nuclei, a

(21) A double bond in the topological theory of molecular structure is evidenced by the charge density along the bond path exhibiting an ellipticity (Bader, R. F. W.; Slee, T. S.; Cremer, D.; Kraka, E. *J. Am. Chem. Soc.* **1983**, *105*, 5061-5068). A bond's ellipticity $\epsilon = (\lambda_1/\lambda_2 - 1)$ where λ_1 and λ_2 are the two negative curvatures of ρ (the curvatures perpendicular to the bond path) at the bond critical point. For a bond with π character, charge density is preferentially disposed in the plane of the " π orbitals" and the magnitude of the corresponding curvature $|\lambda_2|$ is less than $|\lambda_1|$. The ellipticity, which is zero for a bond with no " π character" thus measures the deviation of the charge distribution of a bond path from axial symmetry. In SO₂ the value of ρ at the bond critical point is 0.294 au and $\epsilon = 0.199$ with the soft curvature λ_2 directed along an axis perpendicular to the plane of the nuclei—as anticipated on the basis of an orbital model of the double bonds in SO₂.

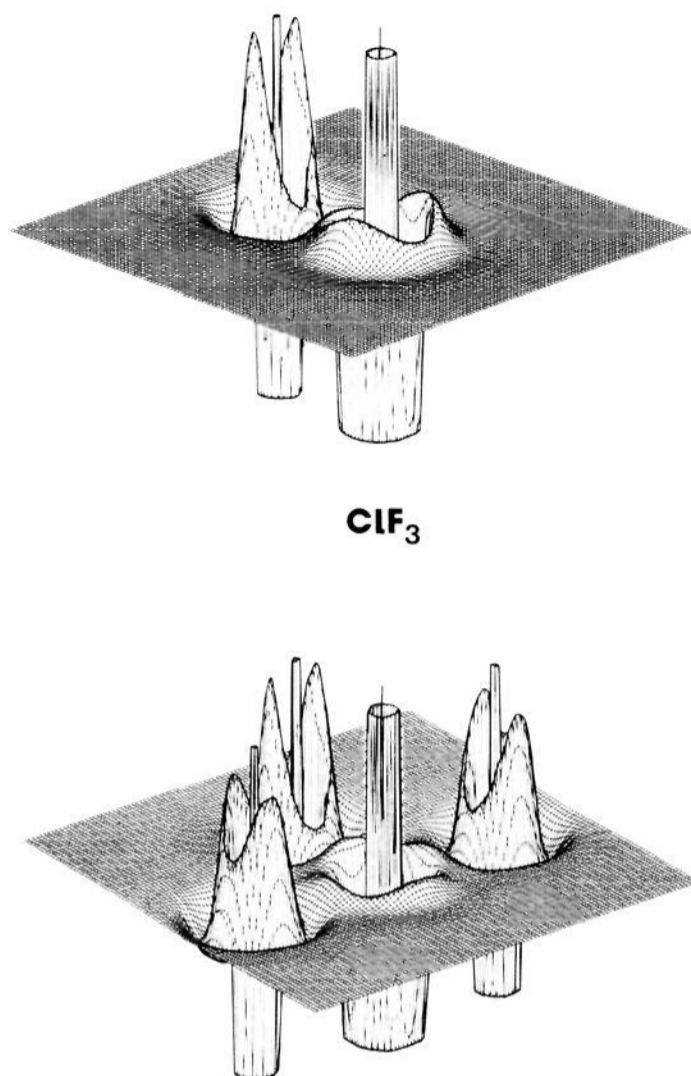


Figure 4. A display of the negative of the Laplacian of ρ for two planes of ClF_3 . The equatorial plane (top) shows the presence of two nonbonded and one bonded concentration of charge in the valence shell of the Cl atom. (Note the presence of three quantum shells for the Cl atom as evidence by three regions of charge concentration and three of charge depletion in $-\nabla^2\rho$.) The plane containing the two axial as well as the equatorial F atoms exhibits three bonded charge concentrations in the valence shell of Cl and another view of the (3, -1) saddle point in $-\nabla^2\rho$ between the two nonbonded concentrations. Thus the Cl atom in ClF_3 possesses two nonbonded and three bonded concentrations of charge in its valence shell.

reflection of the ellipticity of the $\text{S}=\text{O}$ bond (see ref 21). The boundary of one of these bonded charge concentrations does in fact encompass a larger area of this surface than does that of the nonbonded charge maximum (see Table III). The molecules $:\text{SF}_4$ and $\text{O}=\text{SF}_4$, to be considered later, allow the same comparison and yield the same results.

Valence-Shell Charge Concentrations with Five Maxima. The molecules ClF_3 and SF_4 possess five electron pairs in the valence shells of the chlorine and sulfur atoms with the trigonal bipyramid as the most probable arrangement for these pairs. The molecule ClF_3 is "T-shaped" with the nonbonded pairs occupying two of the less crowded equatorial positions. The single nonbonded pair in SF_4 is also assigned an equatorial site, thus accounting for the bisphenoid geometry of this molecule.

Table IV summarizes the properties of the local charge concentrations in the valence shell of the chlorine atom in ClF_3 for the equilibrium geometry and for two higher energy geometries obtained by assigning the fluorine atoms the three equatorial sites to yield a planar geometry, or one axial and two equatorial sites to yield a tripod-like geometry. The bond lengths and bond angles were obtained from a totally unconstrained calculation for the lowest energy "T-shaped" geometry from a calculation constrained to be planar and finally from a calculation in which the only constraint was that one FCIF bond angle be fixed at 120° . The unconstrained calculation yielded an energy -757.03423 au with axial and equatorial bond lengths of 1.682 and 1.607 Å, respectively, and an FCIF angle of 85.36° , in fair agreement with the experimental values²² (in the same order) of 1.70 Å, 1.60 Å, and

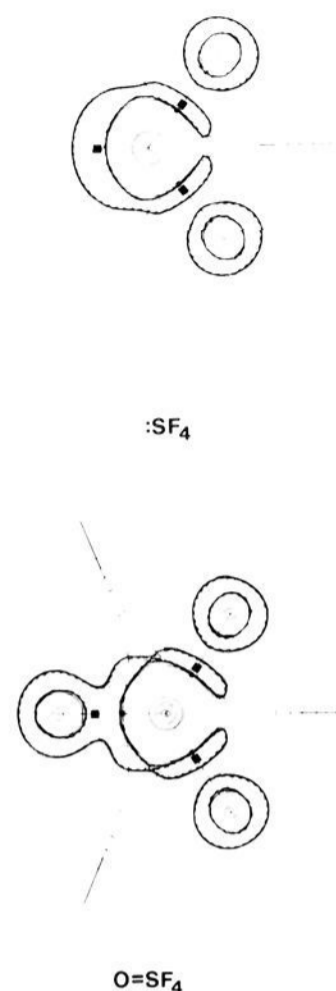


Figure 5. Contour maps of $\nabla^2\rho$ for the equatorial planes of SF_4 and SF_4O . The positions of the local charge concentrations in the valence shells of the sulfur atoms are indicated by solid squares. In this plane there are two bonded and one nonbonded concentrations of charge in SF_4 and three bonded concentrations in SF_4O , one corresponding to the two bonded pairs in the double bond to oxygen. Note that the single charge concentration on the $\text{S}=\text{O}$ bond is within the valence shell of the oxygen atom.

87.5° . The planar geometry possesses a relative energy of $+45.7$ kcal/mol and a bond length of 1.709 Å. The tripod geometry possesses a relative energy of $+63.0$ kcal/mol, axial and equatorial bond lengths of 1.678 and 1.718 Å, respectively, and an axial-equatorial bond angle of 80.6° .

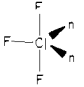
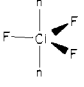
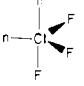
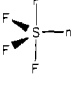

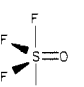

In each case there are five local charge concentrations present in the valence shell of the chlorine atom (see Figure 4). In the equilibrium geometry the size and magnitude of the charge concentrations on chlorine decrease in the order: nonbonded > equatorial bonded > axial bonded. The angle between the two equatorial nonbonded maxima is relatively large and equal to 148° while the axial bonded-nonbonded angle is opened to 97° . In the two geometries of higher energy the smallest of the $n\text{Clb}$ angles is 90° or less, with the smallest angle belonging to the geometry of highest energy. In all geometries, except planar ClF_3 , the smallest intermaxima angle is a bClb angle. All of these observations are in accord with the VSEPR model of molecular geometry.

The calculated equilibrium geometry and energy for SF_4 using the 6-21G* basis set (with experimental values²³ in parentheses) are as follows: equatorial ($\equiv\text{e}$) and axial ($\equiv\text{a}$) bond lengths 1.556 Å (1.545 Å) and 1.623 Å (1.646 Å), $\angle\text{F}_\text{e}\text{SF}_\text{e} = 102.6$ (101.5°), $\angle\text{F}_\text{a}\text{SF}_\text{e} = 86.6^\circ$, $\angle\text{F}_\text{a}\text{SF}_\text{a} = 169.2^\circ$ (173.1°), and $E = -794.56437$ au. As it is in ClF_3 , the angle between an equatorial and an axial fluorine is less than 90° . A second calculation for which the geometry was constrained to C_{3v} symmetry (the nonbonded electron pair is placed in an axial position) yielded an energy 32.9 kcal/mol above that of the equilibrium geometry and the following optimized geometrical parameters: equatorial and axial bond lengths of 1.616 and 1.587 Å, respectively, $\angle\text{F}_\text{e}\text{SF}_\text{e} = 118.6^\circ$, and $\angle\text{F}_\text{e}\text{SF}_\text{a} = 83.1^\circ$.

(22) Smith, D. F. *J. Chem. Phys.* **1953**, *21*, 609-614.

(23) Tolles, W. M.; Gwinn, W. D. *J. Chem. Phys.* **1962**, *36*, 1119-1121.

Table IV. Bonded and Nonbonded Charge Concentrations in ClF_3 , SF_4 , SF_4O , and ClF_5

molecule and geometry	bond	bonded charge concentrations					nonbonded charge concentrations					net charge on F or O	
		$r_A, \text{\AA}$	$\nabla^2\rho, \text{ au}$	area, \AA^2	$\mu_3, \text{ au}$	$\angle b_aAb_e, \text{ deg}$	$\angle nAb, \text{ deg}$	$r_A, \text{\AA}$	$\nabla^2\rho, \text{ au}$	area, \AA^2	$\mu_3, \text{ au}$		$\angle nAn, \text{ deg}$
ClF_3	equatorial (e)	0.670	0.595	0.66	23.1								-0.30
	axial (a)	0.687	0.319	0.41	14.6	83.6	96.5	0.605	1.58	1.52	61.9	147.8	-0.52
ClF_3	equatorial	0.661	0.374		21.2	120 (b_eAb_e)	90.0						
	axial							0.601	1.787		68.7	180.0	
ClF_3	equatorial	0.663	0.428		20.9	73.1	76.5	0.607	1.529		59.5		
	axial	0.672	0.526		19.7		139.3	0.605	1.635		62.5	134.2	
SF_4	equatorial	0.707	0.342	0.94	21.5		129.7	0.666	0.999	1.90	30.7		-0.71
	axial	0.726	0.268	0.49	15.6	84.5	98.6						-0.74
SF_4	equatorial	0.714	0.262		17.7		99.3						
	axial	0.713	0.410		19.6	80.7	180.0	0.667	1.033		30.8		
SF_4O	equatorial	0.705	0.381	0.89	21.9			double bond charge concentration on O ^a				-0.70 (F)	
	axial	0.715	0.381	0.71	19.1	83.0	101.7 (b_oSb_e)	0.463 ^a	1.175 ^a	2.06 ^a	30.8 ^a		-1.29 (O)
ClF_5	single short Cl-F bond	0.653	0.866	0.78	29.4		180.0	0.600	1.900	1.35	69.9		-0.30
	four long Cl-F bonds	0.662	0.619	0.64	23.8	82.8	97.2						-0.44

The charge distributions of both geometries exhibit five local charge concentrations in the valence shell of sulfur, four of which are bonded and one nonbonded (see Figure 5). The same observations regarding the relative properties of the equatorial and axial bonded maxima are obtained for the equilibrium geometry of SF_4 as are found for the equilibrium geometry of ClF_3 ; the equatorial bonded maxima are of greater magnitude and are more tightly bound (r_s is smaller and μ_3 larger) than are the axial bonded maxima. Just the reverse is found for the higher energy C_{3v} geometry. The smallest intermaxima angle in the valence shell of sulfur in the equilibrium geometry is the one between an axial and an equatorial bonded charge concentration. Its value is 84.5° and there are four such angles. The smallest nonbonded-bonded angle of 99° is formed with the two axial bonded maxima. In the C_{3v} geometry the same nonbonded-bonded angle is formed with the three equatorial bonded maxima. However, to accord this identical separation between the nonbonded and adjacent bonded maxima in the C_{3v} geometry, the angle between the three equatorial bonded maxima and the single axial bonded maximum is reduced to only 81° . Thus the smallest angles between the local charge concentrations in the valence shell of the sulfur atom are found in the geometry of highest energy.

The geometry of SF_4O is also related to the trigonal-bipyramidal most probable arrangement of electron pairs by VSEPR theory. In this case the two pairs forming the double bond to oxygen are considered to occupy a single site, as in SO_2 . The results recorded for this molecule in Table IV were obtained using the 6-21G* basis set. The energy and optimized geometrical parameters (with the

experimental values²⁴ in parentheses) are: $E = -869.29824 \text{ au}$, $R(\text{S}=\text{O}) = 1.411 \text{ \AA}$ (1.413), $R(\text{F}_e-\text{S}) = 1.549 \text{ \AA}$ (1.550), $R(\text{F}_a-\text{S}) = 1.582 \text{ \AA}$ (1.583), $\angle \text{F}_e\text{SF}_e = 114.1^\circ$ (114.9°), $\angle \text{OSF}_a = 98.5^\circ$ (97.8°). The bond angle between an axial and an equatorial fluorine is smaller in SF_4O than it is in SF_4 , 85.4° compared with 86.6° . This is accounted for in the VSEPR model by according a larger size to two bonded pairs in a double bond than to a single nonbonded pair of electrons.

There is less differentiation between the axial and equatorial bonded maxima in the valence shell of sulfur in SF_4O than in SF_4 . As in SO_2 , the sulfur-oxygen interaction is very polarized toward the oxygen, and the single bonded maximum on the S-O bond path is in the valence shell of the oxygen atom. The S=O bond in SF_4O exhibits an ellipticity of 0.186, almost the same as that found for the bonds in SO_2 .²¹ As anticipated, the soft curvature λ_2 is directed along an axis perpendicular to the equatorial plane. Again as in SO_2 , the domain of the S-O bonded maximum is contiguous with and covers a relatively large segment of the valence shell of charge concentration on the sulfur atom (see Figure 5). A comparison of contour plots of the Laplacian of ρ for SF_4 and SF_4O in the axial plane, together with the data in Table IV, indicates that the bonded charge maxima for S=O does extend over a greater portion of the sphere of valence charge concentration

(24) Bond lengths from structure (2) of Hencher, J. L.; Cruickshank, D. W. J.; Bauer, S. H. *J. Chem. Phys.* 1968, 48, 518-519. Bond angles from Hedberg, L. 8th Austin Symposium on Molecular Structure, March 3-5, 1980, Abstract MA3.

on sulfur in SF₄O than does the nonbonded charge maximum in SF₄. Thus the angle between the axial and equatorial bonded charge maxima is smaller in SF₄O than it is in SF₄, as is the associated bond angle itself.

Valence-Shell Charge Concentrations with Six Maxima. The final entry in Table IV is for ClF₅. This molecule possesses six pairs of electrons in the valence shell of the chlorine atom, and its geometry, that of a square-based pyramid, is rationalized on the basis of the most probable octahedral arrangement of six electron pairs. The energy and optimized geometry for this molecule, obtained using the 6-21G* basis set, are as follows (with experimental values²⁵ in parentheses): $E = -955.40771$ au; the unique short ClF bond along the fourfold axis and opposed to the nonbonded pair is 1.606 Å (1.62 Å) in length; and the remaining ClF bonds have a length 1.632 Å (1.72 Å), $\angle F_5ClF_1 = 84.4^\circ$ (87.5°).

There are six local concentrations of negative charge in the valence shell of the chlorine atom, five bonded concentrations and one nonbonded. The single nonbonded maximum in ClF₅ is of greater magnitude than are those of the two nonbonded maxima in ClF₃. In ClF₃ and SF₄ the axial fluorides are nearest to the nonbonded maxima and they possess the longest bond lengths. Correspondingly, their bonded maxima are of smaller magnitude and are less tightly bound than are the equatorial maxima. In ClF₅, the four equivalent fluorines are nearest to the nonbonded maxima. They possess the longest bond lengths and their associated bonded maxima on chlorine are of smaller magnitude and are less tightly bound than is that for the single fluorine with the shortest bond length. The bond angle formed by a long and a short bond is calculated to be very similar for ClF₃, SF₄, and ClF₅, $85.5 \pm 1.1^\circ$, as are the corresponding angles between their bonded maxima, $83.6 \pm 0.9^\circ$. In all three molecules the angle between the nonbonded maximum on chlorine or sulfur and the bonded maximum of the longest ligand bond is greater than 90°, ranging from 96.5° in ClF₃ to 98.6° in SF₄. Reference to the average electron populations for the fluorine atoms in these same molecules shows that the fluorine ligands with the longest bond lengths possess the largest net negative charges.

IV. Summary

The number and relative spatial extents of the bonded and nonbonded charge concentrations in the valence shell of an atom as defined by the Laplacian of ρ are in remarkable agreement with the corresponding properties assumed for bonded and nonbonded electron pairs in the VSEPR model of molecular geometry. This agreement does not, however, necessarily imply that the geometry in the neighborhood of a central atom is indeed primarily determined by the repulsions between the electron pairs in its valence shell as is assumed in the VSEPR model. The topological theory of molecular structure enables one to determine the total (Ehrenfest) force acting on an element of electronic charge.^{6,26} This force is expressible in terms of the quantum mechanical stress tensor $\sigma(\mathbf{r})$,

$$\mathbf{F}(\mathbf{r}) = -\nabla \cdot \sigma(\mathbf{r}) \quad (1)$$

In addition, one may also determine the relative magnitudes of the electron–nuclear attractive and electron–electron repulsive contributions to this force. In a future publication, eq 1 will be used to analyze the forces acting on the bonded and nonbonded charge concentrations and in this manner test the basic tenet of the VSEPR model.

V. Charge Concentrations and Models of Bonding and Reactivity

As pointed out in the Introduction, the Laplacian of ρ provides a connection between the form of ρ and the mechanics which

govern this form.⁵ Of particular importance to the present discussion is the appearance of $\nabla^2\rho(\mathbf{r})$ in the local expression of the virial theorem⁶

$$(\hbar^2/4m)\nabla^2\rho(\mathbf{r}) = \mathcal{V}(\mathbf{r}) + 2G(\mathbf{r}) \quad (2)$$

The quantity $\mathcal{V}(\mathbf{r})$ when integrated over the basin of the atom yields $\mathcal{V}(\Omega)$, the virial of all the forces acting on the electronic charge in the basin and surface of an atom in a molecule. When integrated over the total molecule it yields \mathcal{V} , the virial of all the forces exerted on the electronic charge of the molecule. Thus $\mathcal{V}(\Omega)$ and \mathcal{V} are the electronic potential energies for an atom in the molecule and the molecule itself, respectively, and $\mathcal{V}(\mathbf{r})$ is the corresponding potential energy density of the electronic charge element at \mathbf{r} . The quantity $G(\mathbf{r})$ is the kinetic energy density of the electronic charge element at \mathbf{r} . When integrated over an atom or the total system it yields the average electronic kinetic energy of the atom, $T(\Omega)$, or of the total system, T . The integral of $\nabla^2\rho(\mathbf{r})$ vanishes over an atom in a molecule as a direct consequence of its topological definition, as well as over the entire molecule. Hence integration of eq 2 over an atom Ω or over the entire system yields the virial theorem,

$$0 = \mathcal{V}(\Omega) + 2T(\Omega)$$

$$0 = \mathcal{V} + 2T \quad (3)$$

A single theorem applies to an atom in a molecule or to the entire molecule. In eq 2 the sum of the local contributions of the potential and kinetic energy densities to their virial theorem averages is related to a property of the charge density, its Laplacian, $\nabla^2\rho(\mathbf{r})$. While their average values must satisfy the virial theorem, eq 3, their local values in general do not, and instead they satisfy eq 2. Since the potential energy density $\mathcal{V}(\mathbf{r})$ is everywhere negative and the kinetic energy density $G(\mathbf{r})$ is everywhere positive, the sign of the Laplacian of $\rho(\mathbf{r})$ determines which of the two contributions to the virial theorem is dominant in a particular region of space. Since it is also true that electronic charge is concentrated in regions where $\nabla^2\rho < 0$, eq 2 identifies the spatial regions of a molecule where the stabilizing contributions of the potential energy are dominant and simultaneously identifies these regions as those in which electronic charge is locally concentrated.⁵

The property of the Laplacian of ρ , that of determining the regions of concentration and depletion of charge and of relating these to corresponding regions of dominant potential energy decrease and kinetic energy increase, respectively, forms a basis for the classification of atomic interactions. It has been demonstrated that atomic interactions fall into two general classes, closed-shell and shared interactions, each characterized by a particular set of mechanical properties. Interactions resulting from the sharing of charge density between atoms, covalent and polar bonds, are caused by a contraction of the charge density toward the line of interaction linking the nuclei. The negative curvatures of ρ (those perpendicular to the interaction line) are dominant, electronic charge is concentrated in the internuclear region, and $\nabla^2\rho < 0$. These interactions are characterized by the large negative value of the potential energy in the internuclear region. Interactions between closed-shell atoms as found in noble gas repulsive states, in ionic bonds, in hydrogen bonds, and in van der Waal's molecules are governed by the contraction of the charge density toward each of the interacting nuclei. Thus one finds the positive curvatures of ρ (those parallel to radial lines originating at a nucleus) to be dominant in these interactions, electronic charge is depleted in the interatomic surface, and $\nabla^2\rho > 0$. The mechanics are characterized by the relatively large value of the kinetic energy, particularly the component parallel to the interaction line. In the closed-shell interactions, the regions of dominant potential energy contributions are separately localized within the boundaries of each of the interacting atoms or molecules. In the shared interactions a region of low potential energy is contiguous over the basins of both the interacting atoms.²⁷

(25) Begun, G. M.; Fletcher, W. H.; Smith, D. F. *J. Chem. Phys.* **1965**, *42*, 2236–2242.

(26) Bader, R. F. W. *J. Chem. Phys.* **1980**, *73*, 2871–2883.

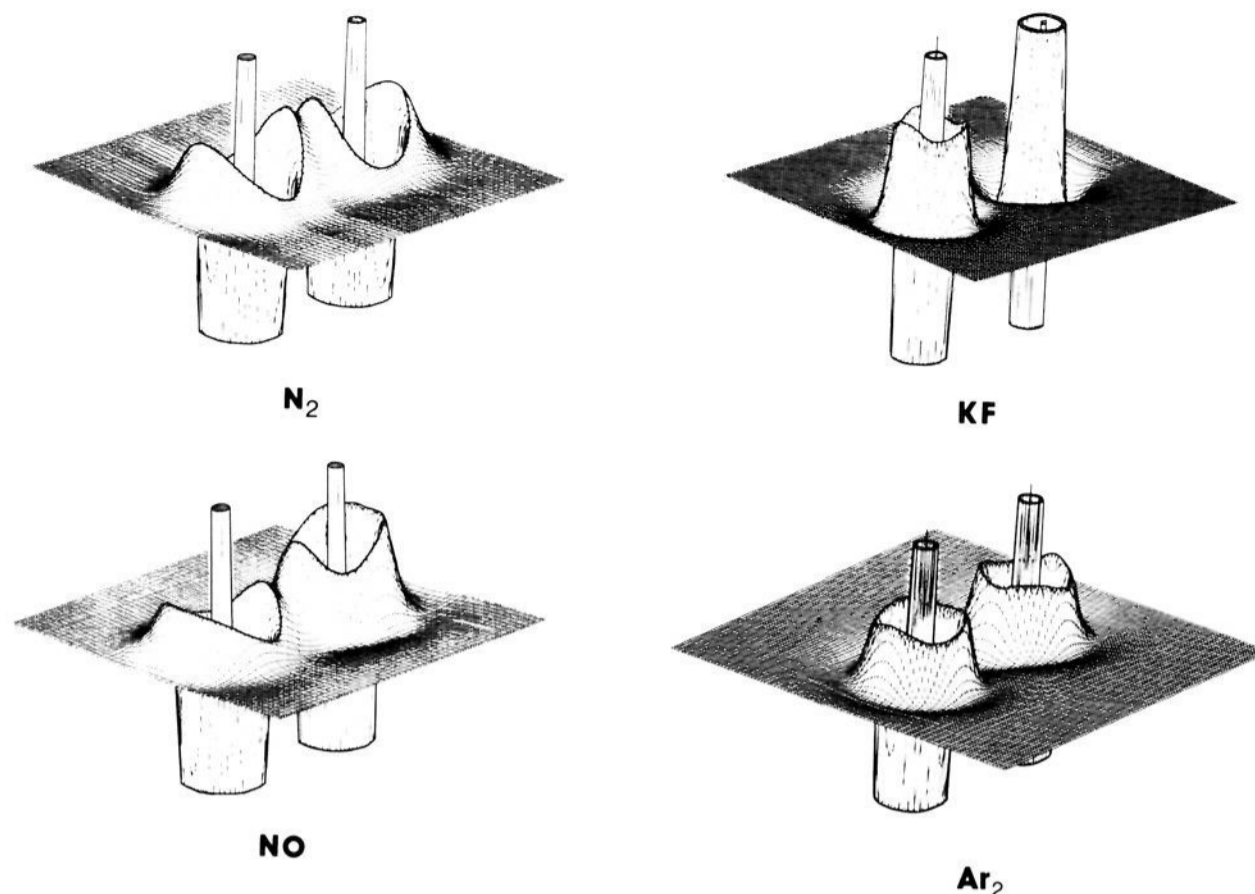


Figure 6. Displays of $-\nabla^2\rho$ for planes containing the nuclei of diatomic molecules. In the examples of shared interactions, N_2 and NO , the valence-shell charge concentrations of the two atoms are joined together and charge is concentrated in the interatomic surface. In the closed-shell interactions, KF and Ar_2 , the valence-shell charge concentrations are separately localized within each atomic basin and charge is depleted in the interatomic surface. In KF the critical point on the atomic boundary is a $(3, +1)$ and $\nabla^2\rho > 0$. In Ar_2 the corresponding critical point is a $(3, +3)$, a local minimum in $-\nabla^2\rho$. Note the similarity in shell structure and polarization of the Laplacian for the K atom in KF with an Ar atom in Ar_2 . K exhibits three rather than four shells, indicating a transfer of its valence charge density to F.

Limiting examples of the two types of atomic interactions are shown in Figure 6. The molecules N_2 and NO illustrate shared interactions. In all of these molecules $\nabla^2\rho < 0$ over the binding region of each interacting pair of nuclei. Thus in shared interactions, electronic charge is concentrated in the internuclear region as a result of the contractions of ρ toward the bond path, and this concentration of charge extends over the atomic basins of both nuclei; the result is a fusion of the valence-shell charge concentrations of the two interacting atoms. In N_2 , for example, the two bonded maxima in $-\nabla^2\rho$ of magnitude 3.677 au are linked by a $(3, -1)$ critical point where $-\nabla^2\rho = 3.050$ au. Each N atom also possesses a nonbonded maximum in $-\nabla^2\rho$ of magnitude 3.176 au. In terms of the Hellmann–Feynman forces exerted on the nuclei, it is the shared concentration of charge which exerts the net attractive forces on the nuclei for $R > R_e$ and balances the nuclear force of repulsion at R_e .⁵ In the closed-shell interactions illustrated by Ar_2 and KF in Figure 6, the region of the interatomic surface is one of charge depletion, and the valence-shell charge concentrations are separately localized in each atomic basin yielding shell-like structures similar to those found in an isolated atom or ion. Clearly such an interaction can result in a bound or unbound state depending upon the direction of polarization of each atomic charge distribution. The directions of these polarizations of the total density are apparent in the Laplacian dis-

tributions of ρ . The Laplacian map for Ar_2 shown in Figure 6 shows the existence of a nonbonded charge maximum on each argon atom of magnitude 1.382 au. The map also indicates that charge is depleted from the region between the nuclei (where $-\nabla^2\rho$ exhibits a local minimum) to a greater extent than it is from the nonbonded region of each nucleus. Thus the net forces on the nuclei are repulsive in accordance with the unbound nature of this state. Elementary considerations show that for an ionic molecule such as KF to achieve electrostatic equilibrium the charge distributions of both the anion and cation must be polarized in a direction counter to the direction of charge transfer.²⁹ The cationic nucleus is attracted by the net negative field of the anion, and the charge distribution of the cation must polarize away from the anion to balance this attractive force. The anionic nucleus is repelled by the net positive field of the cation, and the charge distribution of the anion must polarize toward the cation to balance this repulsive force. Such polarizations are evident in the Laplacian map of KF for which the net charges on the atoms are ± 0.93 e. The potassium *ion* is isoelectronic with an argon atom and the Laplacian of ρ for K in KF including its back-polarization as required for equilibrium in ionic binding is indeed structurally similar to that for an Ar atom in Ar_2 . In K of KF the nonbonded maximum in $-\nabla^2\rho$ is of greater magnitude, 2.376 au, than is its bonded maximum of magnitude 2.016 au. The Laplacian of ρ on the bonded side of the F in KF shows a distinct polarization toward the cation. In ionic systems the nearly complete transfer of the valence density from one atom to the other yields two closed-shell structures, and both nuclei are bound by the net negative electric field exerted by the inwardly polarized charge concentrated within the basin of the anion.^{5,29}

We now illustrate that the regions of charge concentration and charge depletion as defined by the Laplacian of ρ serve to identify the sites of electrophilic and nucleophilic attack. Figure 7 displays the Laplacian of ρ for two planes of the formamide molecule. As anticipated, the keto oxygen possesses two nonbonded charge concentrations in the plane of the nuclei. The doubly bonded nature of the CO link is evidenced in a large ellipticity³⁰ for this

(27) The characteristic behaviors of the potential and kinetic energy densities for shared and closed-shell interactions were made first for H_2 (a shared interaction) and He_2 (a closed-shell interaction) by Bader and Preston.²⁸ The accumulation of charge in the binding region of H_2 resulting from the dominant contractions in ρ perpendicular to the bond path leads to a softening of the parallel curvature of ρ and to a gross reduction in the corresponding parallel component of the kinetic energy density. These observations have now been shown⁵ to be general for shared interactions. Thus as shown by eq 2, since $\nabla^2\rho(r) < 0$ for shared interactions, the potential energy density is dominant over the binding region and the kinetic energy per electron is absolutely small as a result of the near vanishing of its parallel component. In He_2 , a closed-shell interaction, charge density is removed from the interatomic surface as a result of the dominant contraction of ρ toward each nucleus, $\nabla^2\rho > 0$ and by eq 2, and the interaction is dominated by the kinetic energy contributions. In such a situation the parallel curvature of ρ is large as is the corresponding parallel component of the kinetic energy density and the kinetic energy per electron is absolutely large.^{5,28}

(28) Bader, R. F. W.; Preston, H. J. T. *Int. J. Quantum Chem.* **1969**, *3*, 327–347.

(29) Bader, R. F. W.; Henneker, W. *J. Am. Chem. Soc.* **1965**, *87*, 3063–3068.

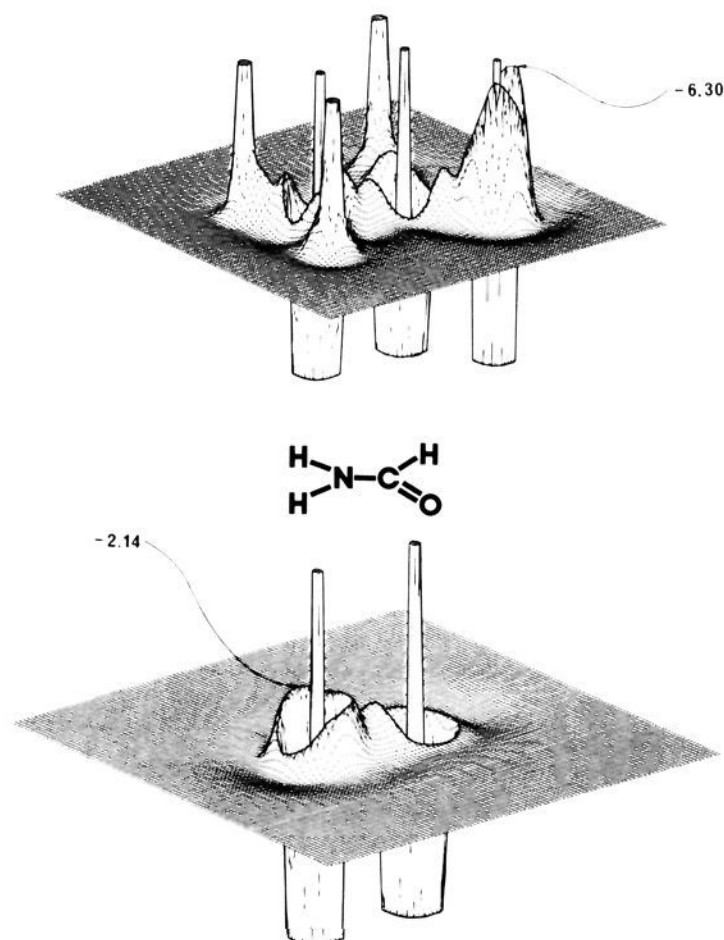


Figure 7. Displays of $-\nabla^2\rho$ for the formamide molecule in the plane containing the nuclei and in the perpendicular plane along the N-C bond axis. The largest valence-shell charge concentrations are found in the nonbonded region of the oxygen atom. While the carbon atom exhibits a shell of charge concentration (both planes show a "lip" around the inner shell region of charge depletion), $\nabla^2\rho$ is actually positive over much of this shell in the perpendicular plane; i.e., only the curvature of $-\nabla^2\rho$ along a radial line out from the C nucleus is negative, and the two curvatures tangent to the surface are positive.

bond equal to 0.433 with its major axis perpendicular to the plane of the nuclei. Thus there is a preferential delocalization of the charge density into the " π " plane. This delocalization extends to the CN bond which also exhibits an ellipticity of 0.013 with a corresponding major axis. The nitrogen atom exhibits two nonbonded charge concentrations in this π plane, but they are only one-third the size of the nonbonded concentrations on the oxygen atom. Thus formamide should protonate at O rather than N as is found experimentally³¹ and as is also predicted on the basis of electrostatic potential maps.^{32,33}

Shown in Figure 8 is a contour map of the Laplacian of ρ for formaldehyde. The Laplacian distribution for the carbonyl group in this molecule is similar in its characteristics to that in formamide. In both molecules the valence-shell charge concentration of the carbonyl carbon exhibits pronounced regions of charge depletion ($\nabla^2\rho > 0$) above and below the plane of the nuclei as a result of the charge transfer to the keto oxygen. Reference to the three-dimensional display for formamide indicates that the radial curvature of $-\nabla^2\rho$ is negative for the valence shell of the carbonyl carbon and that this atom still possesses a surface in which $-\nabla^2\rho$ is a maximum in all radial directions from the carbon nucleus. The two π -type regions of charge deficit on carbon, however, exhibit (3, +1) critical points in $-\nabla^2\rho$. Thus the remaining two curvatures are positive, $-\nabla^2\rho$ is a minimum in the

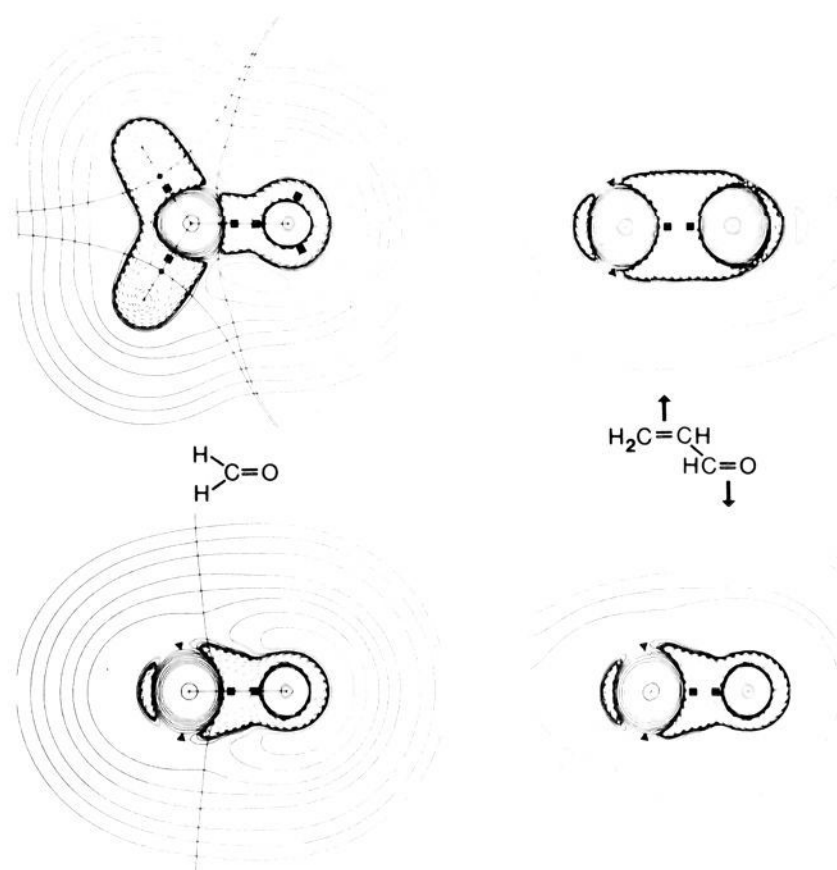


Figure 8. Contour plots of $\nabla^2\rho$ for two planes of formaldehyde, one being the plane containing all the nuclei, the other a plane perpendicular to this and along the C=O axis. Similar plots are shown for planes containing the C=C and C=O bonds of acrolein, perpendicular to the plane of the nuclei. In formaldehyde the top diagram shows the positions of the three bonded charge concentrations (solid squares) in the valence shell of a carbonyl carbon and the single bonded and two nonbonded concentrations in the valence shell of a carbonyl oxygen. The interatomic surfaces and bond critical points are also shown for formaldehyde. The lower diagrams show the two (3, +1) critical points (denoted by solid triangles) which determine the sites of nucleophilic attack at a carbonyl carbon. The positions of the same critical points are indicated on the β carbon and carbonyl carbon of acrolein.

surface of charge concentration, and charge is locally depleted in the surface in the neighborhood of these two critical points. Thus the valence-shell charge concentration of a carbonyl carbon atom exhibits three bonded maxima in the plane of the nuclei and two critical points above and below this plane at which charge is concentrated locally in the radial direction, but depleted in directions perpendicular to the radial direction, i.e., depleted in the surface of charge concentration.

Such (3, +1) critical points correlate with centers of nucleophilic attack. In CH_2O and H_2NCHO the (3, +1) critical points on the carbonyl carbons form angles with the C=O bond axis of 111° and 109° , respectively. Thus a nucleophile is predicted to approach a carbonyl carbon from above or below the plane of the nuclei along a path forming an angle of $\sim 110^\circ$ with the C=O bond axis. The carbonyl carbon of acetaldehyde exhibits the same pattern of critical points in its valence-shell charge concentration. Each (3, +1) critical point forms an angle of 110° with the C=O bond axis, but in addition, is tilted 1.5° out of the perpendicular plane away from the methyl group. What could be interpreted as a steric effect in determining a reaction coordinate is already present as an electronic effect in the unperturbed molecule.

Burgi and Dunitz³⁴ in the "structure-correlation" method consider the relative geometries of two neighboring fragments found in a number of crystal structures as providing snapshots of nuclear configurations along a portion of the coordinate leading to their reaction with one another. For example, from crystal structures containing an amino nitrogen (the nucleophile) in the proximity of a carbonyl group, they find only a small deviation of the $\text{N}\cdots\text{C}=\text{O}$ "approach" angle from its average value of 110° for a range of N \cdots C separations. Assuming this angle to be determined primarily by the local forces acting between the amino and carbonyl fragments, these observations are interpreted as

(30) The results for formamide, acetaldehyde, and formaldehyde are calculated for their optimized geometries using the 6-31G** basis set. The results also given in this section for acrolein were obtained using the 4-31G* basis set.

(31) Birchall, T.; Gillespie, R. *J. Can. J. Chem.* **1963**, *41*, 2642-2650.

(32) Bonaccorsi, R.; Pulman, A.; Scrocco, E.; Tomari, J. *Theor. Chim. Acta* **1972**, *24*, 51-60. Pullman, A. In "Chemical and Biochemical Reactivity"; Bergmann E. D., Pullman, B. Eds.; D. Reidel: Dordrecht, Holland, 1974.

(33) For recent reviews see: (a) Scrocco, E.; Tomasi, J. *Adv. Quantum Chem.* **1978**, *11*, 116-193. (b) Politzer, P.; Daiker, K. C. In "The Force Concept in Chemistry"; Deb, B. M. Ed.; Van Nostrand-Reinhold: New York, 1981; Chapter 7.

(34) Burgi, H. B.; Dunitz, J. D. *Acc. Chem. Res.* **1983**, *16*, 153-161.

implying a preferred angle of $\sim 110^\circ$ for the approach of a nucleophile to a carbonyl carbon. This conclusion is in agreement with the predictions made on the basis of the properties of the valence-shell charge concentration for a carbonyl carbon. Clearly, Laplacian maps may also be used to rationalize and predict preferred inter- and intramolecular geometrical parameters of molecular crystals.

Electrostatic potential maps have been used to predict the sites of electrophilic attack. It has been found, however, that the positive potentials exhibited by such maps are not necessarily indicative of a corresponding affinity for nucleophiles. Recently Politzer et al.³⁵ have found that if the geometry of the system is distorted in the manner amenable to the approach of the nucleophile, a positive channel is present in the potential map leading to the electrophilic center. Politzer et al. consider acrolein, an α,β -unsaturated carbonyl compound which may in principle undergo nucleophilic attack at either the carbonyl or β -carbon atoms. By considering two distorted geometries corresponding to tetrahedral approach angles at these two atoms, they find a pronounced positive channel in the electrostatic potential for the carbonyl carbon but not for the β -carbon. This result is in agreement with the observation that, for α,β -unsaturated aldehydes, nucleophiles react predominantly at the carbonyl carbon.³⁵

Similar conclusions can be reached by considering the Laplacian distribution of ρ for the equilibrium geometry of acrolein. Figure 8 illustrates the Laplacian of ρ for this molecule in the plane perpendicular to the plane of the nuclei for the α,β -unsaturated and carbonyl bonds. Each of the framework bonds exhibits an ellipticity, all with their major axes perpendicular to the plane of the nuclei. (The ϵ values are: $C_\beta=C_\alpha$, 0.40; $C_\alpha-C$, 0.08; $C=O$, 0.09). Thus charge from the $C=C$ and $C=O$ double bonds is delocalized in the π plane into the intervening $C_\alpha-C$ bond. The β and carbonyl carbons exhibit (3, +1) critical points above and below the plane of the nuclei in regions of local charge depletion in their valence shells. The minimum in $-\nabla^2\rho$ is greater for the carbonyl carbon, $\nabla^2\rho = 0.100$ au, than it is for the β carbon, $\nabla^2\rho = 0.062$ au, indicating preferential nucleophilic attack at the former atom. The (3, +1) critical points on the carbonyl carbon form angles with the $C=O$ bond axis of 107° . The angles formed by the corresponding critical points on the β carbon with the $C=C$ bond axis are 114° .

The above examples illustrate what is to be further demonstrated in future reports for other types of reactions—that regions of nonbonded charge concentration and charge depletion as determined by the Laplacian of ρ , respectively, identify the sites of electrophilic and nucleophilic attack in a molecule, electrophilic

aromatic substitution, for example. Unlike an electrostatic potential map, the Laplacian of ρ is a local function and rapidly calculated. The local maxima and minima in the surface of charge concentration for an atom are precisely located, thereby determining the centers and relative orientations of attack and their corresponding values of $\nabla^2\rho$ quantitatively determined, thereby providing a measure of the susceptibility of a center to electrophilic or nucleophilic attack. An electrostatic map measures only the classical electrostatic contribution to the potential at a point in space. Equation 2 relates $\nabla^2\rho$ to the total electronic potential energy density $\mathcal{V}(\mathbf{r})$, a density which in turn is related to the virial of the Ehrenfest force $-\nabla\cdot\sigma(\mathbf{r})$ acting on an element of charge. This quantum force, as well as containing the two contributions given by the gradient of the electrostatic potential, also contains the forces arising from the exchange and correlative interactions between the electrons;^{5,7} i.e., it determines the total force acting on an element of electronic charge.

The Laplacian of ρ may also be used to quantify the concept of "hard and soft" bases or nucleophiles.³⁶ In carbon monoxide, for example, both the carbon and oxygen atoms exhibit nonbonded charge maxima. The maximum on oxygen is relatively tightly bound, $r_0 = 0.34$ Å, of considerable magnitude, $|\nabla^2\rho| = 5.18$ au, and of limited radial extent. Its radial curvature is 555 au, and the width along the molecular axis over which $\nabla^2\rho$ is negative equals 0.2 Å. The corresponding maximum on carbon is 0.46 Å from the nucleus, of smaller magnitude, $|\nabla^2\rho| = 1.41$ au, and of much greater radial extent. The radial curvature $\mu_3 = 63.4$ au, and its width is 0.4 Å. The carbon monoxide molecule can act as a hard or a soft base, and the two behaviors are clearly distinguished by the differing characteristics of the nonbonded charge maxima in this molecule as defined by the Laplacian of ρ . With a quantitative classification scheme based upon the properties of the Laplacian of ρ , one might hope to obtain predictions of chemical reactions on the basis of hard maxima reacting with hard holes and soft maxima with soft holes. Molecules approaching one another do not "see" average atomic charges (however they are calculated). Nor do they "see" the electrostatic potential. They just might "see" mutually aligned centers of charge depletion and charge concentration as determined by the Laplacian of ρ .

Acknowledgment. We wish to thank Professor R. J. Gillespie of this Department for many useful discussions and for his constant encouragement in our search for evidence of "lone pairs" in the properties of the electronic charge distribution. We also thank Mr. D. Morgan for the modification of existing programs and the writing of new ones as required for this research.

(35) Politzer, P.; Landry, S. J.; Warnheim, T. *J. Phys. Chem.* **1982**, *86*, 4767-4771.

(36) Pearson, R. G. *J. Am. Chem. Soc.* **1963**, *85*, 3533-3539; *Science (N.Y.)* **1966**, *151*, 172-177.